# Fe nanowires on vicinal Cu surfaces: *Ab initio* study

D. Spišák* and J. Hafner
*Institut für Materialphysik and Center for Computational Materials Science, Universität Wien, Sensengasse 8/12, A-1090 Wien, Austria*
(Received 13 December 2001; revised manuscript received 14 March 2002; published 24 May 2002)

Local-spin-density-functional theory is applied to describe the structural and magnetic properties of iron wires consisting of chains of single atoms. It is shown that an unsupported isolated wire is unstable with respect to both dimerization and bending. The preferential positions of wires grown on stepped Cu(11$n$) surfaces are the inner corner sites of the steps. From the total energy differences the effective intrachain and interchain exchange constants are estimated for wires at different distances. In all cases the resulting magnetic order is ferromagnetic. Regarding an array of magnetic moments arranged in parallel rows as a quasi-two-dimensional $XY$ ferromagnet subject to uniaxial anisotropy with the easy axis parallel to the surface, we find the Curie temperature of Fe wires on Cu(117) using Monte Carlo simulation. Our results are consistent with a critical behavior characteristic of the $XY$ model.

DOI: 10.1103/PhysRevB.65.235405 PACS number(s): 73.22.−f, 75.40.Cx, 75.75.+a

## I. INTRODUCTION

The advances made during the last two decades in preparing and studying magnetic overlayers and multilayered systems have brought about the discovery of a number of new fundamental physical phenomena such as, for instance, induced magnetization in nonmagnetic metals, oscillatory magnetic coupling, or giant magnetoresistance.[1] Currently, these two-dimensional materials are being integrated into electronic devices. Going down by one dimension, linear nanostructures have recently attracted much attention both for basic research and for envisaged applications in technology. Various techniques have been used for the production of long and regular wires. Standard optical lithography allows patterning of structures down to a scale of about 200 nm. Electrodeposition inside the void spaces of anodic aluminum oxide or track-etched polymer membranes is at present the method of choice for producing arrays of wires of diameters down to about 10 nm.[2,3] Single metal wires of a similar diameter could be prepared by deposition onto nanotubes buffered by a Ti layer.[4] Monatomic chains or stripes of subnanometer width have been fabricated by molecular-beam epitaxy on ordered stepped surfaces, which are distinguished by an inherent periodic one-dimensional pattern.[5–10] In the appropriate temperature range, deposited atoms adsorb preferentially on step ledges and their mobility along the ledge is enhanced, these are crucial preconditions for the uniformity of the nanowires. This widely applicable technique permits the preparation of large-area nanostructured samples of outstanding quality and, moreover, one of the important structural parameters, the interwire distance, can be tuned simply by changing the miscut angle. Examples of nanowires grown by self-assembly on vicinal surfaces include stripes of Fe on stepped W(110),[5] Cu on stepped Mo(110) and W(110),[6] Fe on stepped Cu(111),[7] Co on stepped Au(111),[8] Ag, Cu,[9] and Co (Ref. 10) on Pt(997), or Fe stripes on stepped Si(111) substrates.[11]

Till recently, due to large unit cells required for the description of nanostructured surfaces, theoretical studies were feasible merely within semiempirical methods. The increasing performance of computers makes it possible to launch first-principles calculations, which allow to gain more insight into the physical phenomena on an atomistic level than available by experimental techniques. This has been manifested by recent work on magnetism of 4$d$ metallic wires on Ag vicinals.[12] The purpose of the present work is a systematic *ab initio* investigation of the structural and magnetic interactions in Fe chains formed on Cu(11$n$) surfaces. The Cu(11$n$) surfaces belong to vicinals characterized by (001) terraces $n/2$ atoms wide. The terraces are terminated by straight steps of ⟨110⟩ orientation and separated by {111} microfacets. Our recent calculations of multilayer surface relaxations of Cu(11$n$) and Cu(10$n$) surfaces[13] described correctly the interlayer spacing contraction/expansion trends and we were able to reproduce the measured formation energies of {110}- and {111}-faceted steps.[14]

One-dimensional Fe stripes on vicinal Cu surfaces with (111) terraces and steps aligned along the ⟨110⟩ direction were explored by Shen *el al.*[7] At low coverage nonuniform stripes one to two atoms high and with a width of more than four atom rows, fragmented into (10–20)-nm-long pieces, were observed. Stripe morphology has a significant influence on magnetic properties. Stripes were found to exhibit a ferromagnetic behavior with time-dependent magnetization, which could be explained in terms of a model involving finite interacting blocks of Ising spins, basically the stripes behaved superparamagnetically.

Early stages of the Fe/Cu(100) interface formation with focus on substrates with a high density of steps have been examined by scanning tunneling microscopy.[15] It has been observed that straight steps of an unspecified orientation tend to rearrange into irregular steps, with the longest segments along ⟨110⟩ directions upon deposition of only 0.035 ML of Fe. Hence (11$n$) vicinal surfaces with the steps aligned along the ⟨110⟩ direction can be anticipated as suitable templates for a production of steady monoatomic iron wires.

The outline of the paper is as follows. Section II is devoted to a brief description of the calculational method and setup we have used. We start by presenting the results for single Fe wires in Sec. III, the morphology and magnetic structure of arrays of parallel Fe wires on Cu(11$n$) surfaces are reported in Secs. IV and V. The magnetic phase transition

 

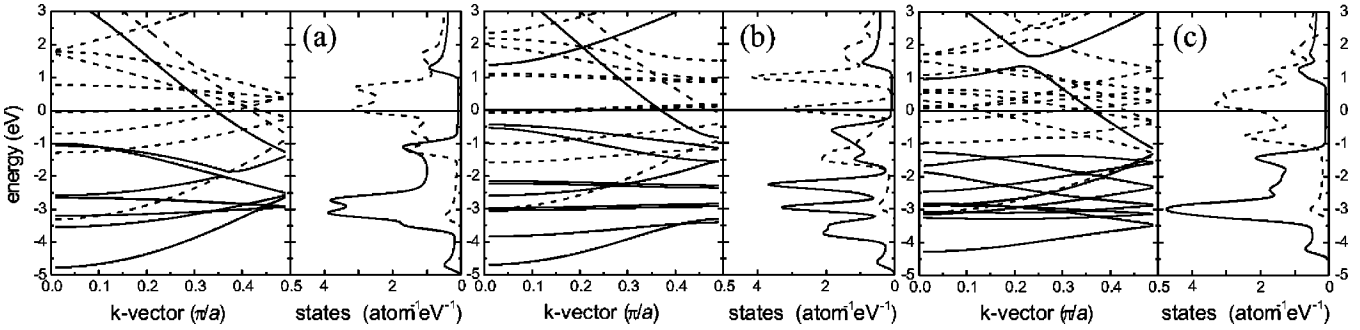


FIG. 1. Band structures and atom-resolved densities of states for Fe chains: (a) undistorted chain, (b) dimerized chain, (c) zigzag-shaped chain with the bond-bond angle of 149°. The solid (dashed) lines depict the majority (minority) spin states. The Fermi energy defines the zero point on the energy scale.

to a paramagnetic state and an adequate estimation of the critical temperature on the basis of numerical simulations is discussed in Sec. VI. Finally, in Sec. VII we summarize our main results and conclude.

## II. COMPUTATIONAL DETAILS

As already noted above, the calculations reported here were performed within the framework of the density-functional theory. We used the Vienna *ab initio* simulation package,[16] VASP, in a projector augmented-wave representation, which is as accurate as the relaxed-core all-electron methods.[17,18] Exchange and correlation effects were described by the functional due to Perdew and Zunger,[19] employing the spin interpolation proposed by Vosko *et al.*[20] and adding generalized gradient corrections.[21] Structural relaxations were performed using a quasi-Newton algorithm, making use of the Hellmann-Feynman forces acting on ions.

The free-standing isolated wires were modeled by periodically repeated slabs 20 Å wide in the $x$ and $y$ directions. The one-dimensional Brillouin zone was sampled by 25 $k$ points. For the $(11n)$ surfaces the supercells were constructed by stacking eight (001) layers, which were in turn rotated by the corresponding miscut angle. The shortest distance from one slab to its nearest image always exceeded 14.7 Å. Some calculations for (117) surfaces were repeated with a shorter distance of 9.4 Å in order to estimate the error bars for differences in total energies for ferromagnetic and antiferromagnetic solutions introduced by the slab geometry, and the differences were never in excess of 1 meV/Fe atom. The Fe atoms were put symmetrically on both sides of the slab. During structural relaxations, undertaken for ferromagnetic Fe/Cu(117) models, the top and bottom eight (117) layers were free to move. Relaxation was stopped when the forces acting on each ion dropped below 0.02 eV/Å. In the interior of the slabs, the interlayer distances were fixed to values corresponding to the calculated Cu lattice spacing of $a=3.637$ Å. The number of $k$ points was chosen according to the requirement that the number of atoms times the number of $k$ points in the irreducible Brillouin zone was always between 300 and 370, and the supercells in our calculations encompassed between 28 and 92 atoms.

## III. FREE-STANDING Fe CHAINS

Before we turn our attention to the realistic case of Fe chains grown on $Cu(11n)$, it is instructive to explore properties of a free-standing Fe wire with a monatomic cross section. Minimization of the total energy with respect to interatomic distance gives an equilibrium bond length of $a_0=2.252$ Å and a magnetic moment of $3.34\mu_B$/atom for parallel magnetic moments, and 2.378 Å and $3.05\mu_B$/atom for alternating magnetic moments. The ferromagnetic configuration is lower in energy by 347 meV/atom. Because in a nonmagnetic wire we obtained $a_0=1.943$ Å (and the energy is higher by 623 meV/atom compared to the ferromagnetic solution), the onset of magnetism is always accompanied by a considerable wire elongation. As one-dimensional metals are unstable with respect to static lattice deformations,[22] we allowed for two conceivable deformations of the chain: Peierls or spin-Peierls dimerization and a formation of a zigzag curve. Both deformations work in favor of lowering the total energy. The modulated interatomic distances in a dimerized chain are $(1\pm0.164)a_0$ and the energy decreases by $-19.7$ meV/atom. For the crooked chain we explored two possibilities.

(i) Every second atom was shifted by the same amount along a direction perpendicular to the wire, imitating a shear deformation. In such a geometry the interatomic bond length elongates with the increasing bending angle. The energy minimum is found for the angle of 149° lower by 54 meV/atom compared to an undistorted wire.

(ii) The bond-bond angle is varied keeping all Fe-Fe bond lengths equal to that calculated for a straight wire. Apparently, this deformation has the greatest effect on a wire—it collapses to a nearly triangular stripe with a bending angle of 68° and an energy gain of 1.01 eV/atom. At a still smaller angle of 55° the magnetic moment drops from about $2.9\mu_B$ to $1.5\mu_B$. This transition from a high-spin to a low-spin state could be an indication that the ferromagnetic state gets unstable and a different magnetic state, e.g., regarding an inherent frustration of an antiferromagnet in a triangular geometry, noncollinear order would develop. We note that all the tackled deformations are confined to a plane and that no structural optimization was carried out.

The analysis of electronic band dispersion and of the den-

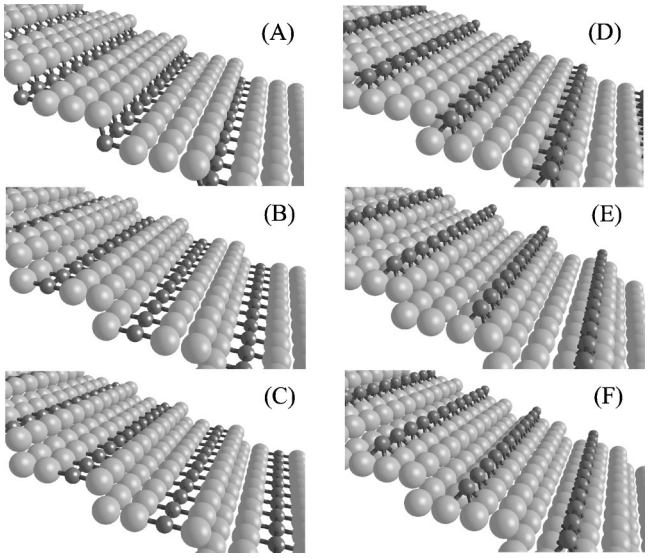


FIG. 2. The oblique view of the surface of structural models representing monatomic Fe chains on Cu(117) substrate, ordered in the sequence of increasing energies; (a) Fe buried below step edge, (b), (c) Fe wires in the terraces, (d) Fe atoms decorating the edge, (e), (f) Fe wires on top of the terraces. The Fe atoms are depicted as smaller darker balls with displayed bonds to the neighbors.

sities of states (DOS), shown in Fig. 1, reveals a nearly half-metallic character of the Fe wire, in which the occupied states in the majority band are separated by about a 2-eV-wide gap from the unoccupied ones, if the minimal DOS of *s* bands in this range is disregarded. The overall stability of the chain is determined by the DOS of the minority *d* electrons near the Fermi level. It can be concluded that upon dimerization, the *d* states of $xy,yz$, and $3z^2-r^2$ symmetry are pushed away from the Fermi level to higher and lower energies, leading to a depletion of electron states just below and above the Fermi level. Allowing a chain bending reduces the DOS at $E_F$ from three to two states per eV, by shifting the $xy$ and $x^2-y^2$ states upwards. Moreover, it is easily seen from the displayed band structures that the magnetic exchange splitting between majority and minority spin bands is large not only for *d* bands but also for *sp* bands. This is in contrast to the Fe crystal, in which the *sp* bands are weakly polarized in opposite direction to the *d* bands.

## IV. Fe CHAINS ON Cu(11*n*) SURFACES

To begin with, we discuss a ferromagnetic array of Fe chains on the Cu(117) substrate. We have considered altogether six different locations of the Fe wires, which are displayed in Fig. 2 and labeled by (a)-(f). This classification will be used throughout the paper. The energies counted from the most stable configuration (a) obtained for a relaxed geometry, the energy gain by relaxation, and the magnetic moments of the relaxed wires are listed in Table I. As can be seen, Fe atoms tend to embed into the Cu substrate and the total energy increases with decreasing Fe-Cu coordination. This provides an indication that Fe-Cu heterobonds are stronger than Cu-Cu bonds. The results for Fe wires resemble those for a complete Fe(001) monolayer placed onto or buried in a Cu(001) substrate. It turned out that such a monolayer prefers to be coated with two Cu overlayers, reducing in this manner the surface energy, because the calculated surface energy of $\gamma$-Fe(001) is higher than that of the Cu(001) surface.[23] Analogous conclusions were drawn for an Fe impurity located near the Cu(001) surface.

TABLE I. Calculated energy differences $\Delta E$ for various relaxed configurations as classified in Fig. 2 with respect to the ground-state configuration (a). $\Delta E_r$ is the change in energy by a relaxation relative to an ideal structure with all positions as in a (117) structure. The magnetic moments of ferromagnetically coupled Fe atoms arranged into chains are provided in the last column.

| Configuration | $\Delta E$ (meV/Fe atom) | $\Delta E_r$ (meV/Fe atom) | $m_{\mathrm{Fe}}^{\uparrow\uparrow}$ |
|---|---|---|---|
| (a) | 0 | −34 | $2.80\mu_B$ |
| (b) | 138 | −47 | $2.91\mu_B$ |
| (c) | 169 | −32 | $2.91\mu_B$ |
| (d) | 262 | −42 | $2.92\mu_B$ |
| (e) | 588 | −120 | $2.93\mu_B$ |
| (f) | 608 | −95 | $2.96\mu_B$ |

Relaxation does not change the order of the most stable configurations, but upon relaxation the chains just above terrace ledges in configuration (e), where nearby atoms are more loosely coupled, reduce their strain more than in case (f) with chains in the middle of a terrace, making configuration (e) after relaxation more stable compared to configuration (f). The lateral and vertical interlayer relaxations of Cu(117), with Cu atom rows replaced by Fe atom rows in the first up to the fourth (117) layer, are presented in Table II. On symmetry grounds, no rearrangement is expected along the step direction. The lateral displacements are rather small. Concerning the vertical relaxations, the step and all terrace atoms relax inwards, whereas the corner atoms exhibit an outward relaxation, meaning that the stepped surfaces flatten by relaxation. It is notable that the vertical relaxations are smallest for the ground-state configuration (a), and a comparison with pure Cu(117) without Fe wires reveals that a chain of Fe atoms fits better into the corner than Cu atoms alone.

The fact that we identify the inner corner sites of the terrace as the preferential position of a wire does not yet mean that it will be realized during a growth process. Previously we have calculated the energy of an Fe adatom on Cu(001), required to trade places with any of its Cu neighbors.[23] The calculated energy barrier of such a process is a sizable $\Delta E \approx 1.45$ eV. For the incorporation of Fe atoms into the (100) terraces, we can safely assume an activation energy of the same order of magnitude. As the exchange mechanism for placing Fe adatoms below the step edge is even more complex, the exchange barrier is likely to be even higher and would be kinetically hindered. For these reasons, if Fe atoms are deposited at low temperatures on a Cu(11*n*) substrate, they are supposed to build rows attached to uphill step edges according to the configuration (d).

TABLE II. Lateral and vertical interlayer relaxations of Cu(117) with Fe nanowires. Lateral relaxations are given in percentages of the ideal bond length 2.572 Å, vertical relaxations along the [117] direction are given in percentages of the interlayer distance 0.509 Å. The second and third columns report the relaxations on a clean Cu(117) surface, the remaining results refer to configurations (a) to (d) shown in Fig. 2.

| Layer | Cu(117) [a] | | (a) | | (b) | | (c) | | (d) | |
|---|---|---|---|---|---|---|---|---|---|---|
| | $x$ | $z$ | $x$ | $z$ | $x$ | $z$ | $x$ | $z$ | $x$ | $z$ |
| 1 | −1.6 | −9.3 | −0.7 | −7.7 | −1.3 | −15.8 | −2.7 | −8.8 | −2.4 | −14.0 |
| 2 | −1.2 | −7.7 | −0.8 | −6.4 | −1.8 | −2.9 | −1.3 | −5.2 | −0.6 | 0.8 |
| 3 | −1.1 | −21.8 | −2.0 | −15.7 | −1.7 | −21.4 | −0.6 | −14.7 | −2.0 | −22.8 |
| 4 | 1.7 | 14.3 | 2.2 | 13.3 | 2.7 | 20.2 | 1.3 | 17.0 | 2.9 | 22.3 |
| 5 | 0.5 | −3.0 | 0.1 | −1.8 | −0.1 | −1.1 | 0.6 | −3.0 | −0.2 | −7.1 |
| 6 | 0.3 | −9.1 | 0.0 | −1.0 | 0.6 | −5.4 | −1.0 | −7.4 | 0.2 | −2.5 |
| 7 | −1.0 | 5.6 | −0.7 | −1.0 | −1.1 | 2.4 | 0.6 | 6.5 | −1.0 | 1.7 |
| 8 | 0.4 | −0.2 | 0.4 | 4.4 | 0.4 | 2.5 | 0.0 | 0.6 | 0.6 | 2.9 |

[a]Reference 13.

## V. MAGNETIC EXCHANGE INTERACTIONS

In the following we want to explore the intrachain and interchain magnetic coupling. Because the structure optimization discussed in the foregoing paragraphs did not lead to any significant variation of magnetic moments, it is acceptable to confine oneself to unrelaxed geometries. The strength of intrachain magnetic coupling can be deduced from the energy difference of ferromagnetically and antiferromagnetically aligned moments along a wire. We have performed such a calculation for a wire in configuration (d) on Cu(117). The effective intrachain coupling constant $J_{\parallel}=140.5$ meV is surprisingly high, in fact one order of magnitude higher than the dominant coupling constants in bulk Fe.[24]

The interchain coupling constants $J_{\perp}$ have been calculated exploiting supercells doubled in the direction perpendicular to the wires, and for parallel and antiparallel alignment of the moments on the two wires on each side of the supercell. With the exception of the wires on a (113) substrate, the interaction couplings are considerably smaller than the intrachain coupling and they vary with the chain-chain distance in a nonmonotonic way, see Table III. Presumably, the source of this variable coupling strength, depending on the interwire distance, is the Ruderman-Kittel-Kasuya-Yosida interaction via intervening substrate $sp$ electrons. In the example of wires on Cu(117) we note that the magnetic coupling strength tends to increase as the wire becomes surrounded by more host Cu atoms, i.e., in the sequence (d) $\rightarrow$(c)$\rightarrow$(a). Oscillations in sign akin to those in the well-studied interlayer exchange coupling in magnetic layers, separated by a nonmagnetic spacer could be anticipated. The coupling periods are determined by the extremal spanning vectors of the Fermi surface in the direction of a layer normal. However, because these vectors do not change with the spacer thickness in multilayers, but do differ for wires on various $(11n)$ surfaces, where they point along the $[nn\overline{2}]$ directions, an oscillatory interwire coupling generally cannot be expected.

In order to check the numerical accuracy of rather tiny exchange couplings, the calculation for the configuration (d) on Cu(117) was repeated with a doubled number of $k$ points in the irreducible Brillouin zone. The obtained inaccuracy in energy difference is as small as 0.1 meV, a value one order of

TABLE III. Interwire coupling constants $J_{\perp}$ and magnetic moments of ferromagnetically ($m_{\mathrm{Fe}}^{\uparrow\uparrow}$) and antiferromagnetically ($m_{\mathrm{Fe}}^{\uparrow\downarrow}$) coupled wires as functions of interwire distance $l$ and the wire location on Cu($11n$) surfaces. For the evaluation of the critical temperature $T_C^I$ in an Ising model, see text.

| Surface | $l$ (Å) | Configuration | $J_{\perp}$(meV) | $m_{\mathrm{Fe}}^{\uparrow\uparrow}$ | $m_{\mathrm{Fe}}^{\uparrow\downarrow}$ | $T_C^I$ (K) |
|---|---|---|---|---|---|---|
| (1 1 3) | 4.066 | (d) | 35.3 | $2.98\mu_B$ | $\pm 2.97\mu_B$ | 2024 |
| (1 1 5) | 6.557 | (d) | 1.3 | $2.97\mu_B$ | $\pm 2.97\mu_B$ | 817 |
| (1 1 7) | 9.092 | (d) | 3.9[a] | $2.95\mu_B$ | $\pm 2.96\mu_B$ | 1040 |
| | | (d) | 4.0[b] | $2.96\mu_B$ | $\pm 2.96\mu_B$ | 1046 |
| | | (c) | 5.1 | $2.90\mu_B$ | $\pm 2.91\mu_B$ | 1111 |
| | | (a) | 5.9 | $2.78\mu_B$ | $\pm 2.79\mu_B$ | 1144 |
| (1 1 9) | 11.644 | (d) | 0.5 | $2.98\mu_B$ | $\pm 2.97\mu_B$ | 684 |
| (1 1 11) | 14.204 | (d) | 3.5 | $3.01\mu_B$ | $\pm 3.01\mu_B$ | 1013 |

[a]Calculated with 5 $k$ points.
[b]Calculated with 10 $k$ points.

magnitude smaller than the energies of interest here. In addition, we investigated a stripe two Fe atoms wide, decorating the steps of a (119) substrate. In this case the interwire coupling between the touching wires is of the same order of magnitude as the intrawire coupling in the longitudinal direction, $J_\perp = 82.8$ meV.

The magnetostatic interaction enforces an in-plane magnetization, however, a sufficiently strong surface- or step-induced anisotropy could induce a resultant magnetization normal to the surface. While a calculation of the step-induced magnetic anisotropy energy is outside the scope of the present paper, the magnetostatic energy is easily evaluated by a direct summation over dipole-dipole pairs. We find that the magnetostatic interaction always works to confine all moments in the same direction along wires. Taking, for example, wires on the (115) surface, the alignment of moments along wires but antiparallel between wires costs an additional magnetostatic energy of 44 $\mu$eV/atom; ferromagnetically and antiferromagnetically coupled wires with the moments oriented across the wires cost 291 $\mu$eV/atom and 359 $\mu$eV/atom, respectively. Upon rotation of the magnetization out of plane, an even larger increase of the magnetostatic energy follows, 381 $\mu$eV/atom in the case of parallel magnetic interwire coupling and 324 $\mu$eV/atom for the antiparallel one. In systems with wider terraces the trends remain the same, but the strength of the magnetostatic coupling decays rapidly. Altogether, it can be concluded that the dipolar interactions favor ferromagnetically ordered arrays of wires with an in-plane magnetization along the wires, and that the interchain magnetic coupling exceeds the dipolar interactions by two orders of magnitude.

## VI. TRANSITION TEMPERATURES

Now we would like to find an estimate of the temperature of the phase transition to a paramagnetic state. In the limit of infinite uniaxial anisotropy, the famous exact solution of the spatial-anisotropic Ising model on a square lattice[25] given by Onsager,

$$\sinh \frac{2J_\parallel}{k_B T_C^I} \sinh \frac{2J_\perp}{k_B T_C^I} = 1, \tag{1}$$

can be applied. The critical temperatures calculated in this way, which have to be considered as the upper bounds, are presented in Table III. A more down-to-earth treatment should allow for uniaxial anisotropies of the order of 1 meV. Assuming the in-plane shape anisotropy, the appropriate description of the system is furnished by the spatial-anisotropic $XY$ model with an uniaxial anisotropy term

$$E = -J_\parallel \sum_{i,\delta_\parallel} \cos(\varphi_{i+\delta_\parallel} - \varphi_i) - J_\perp \sum_{i,\delta_\perp} \cos(\varphi_{i+\delta_\perp} - \varphi_i) - D \sum_i \cos^2(\varphi_i). \tag{2}$$

In this equation, the angle $\varphi_i$ denotes the direction of the classical magnetic moment at a lattice point $i$ relative to step edges, $J_{\parallel(\perp)}$ are the exchange couplings with the nearest neighbors at sites labeled $i+\delta_{\parallel(\perp)}$ along (across) the wire, and $D$ specifies the strength of the single-ion uniaxial anisotropy. Here, positive values of $D$ lead to magnetic moments preferably directed along the wires. With increasing amount of anisotropy the model approaches an Ising system. Analytical studies of the $XY$ model with uniaxial anisotropy do not find any abrupt crossover region, rather they are consistent with a smooth asymptotic approach to the critical temperature of the Ising model.[26,27] We will show that for the weak anisotropies considered by us, the findings are consistent with those expected for an $XY$ model.

The renormalization-group technique applied to the isotropic $XY$ model ($J_\parallel = J_\perp, D = 0$) predicts a peculiar phase transition connected to the dissociation of bound spin vortices.[28] In the thermodynamic limit the existence of a spontaneous magnetization is excluded at any nonzero temperature. Nevertheless, it has been shown[29] that this thermodynamic limit is inaccessible not only in computer simulations but also in experiment, implying the presence of magnetic ordering below the critical temperature. Therefore in the discussion of our data from Monte Carlo simulation, we concentrate on the temperature variation of the average magnetic moment representing the order parameter

$$m = \frac{1}{N} \left\langle \sqrt{\sum_i m_i^2} \right\rangle \tag{3}$$

and mainly on the helicity modulus across the wires,

$$\gamma_\perp = \frac{J_\perp}{N} \left\langle \sum_{i,\delta_\perp} \cos(\varphi_{i+\delta_\perp} - \varphi_i) \right\rangle - \frac{J_\perp^2}{N k_B T} \left\langle \left( \sum_{i,\delta_\perp} \sin(\varphi_{i+\delta_\perp} - \varphi_i) \right)^2 \right\rangle, \tag{4}$$

where $N$ is the number of lattice sites and the angular brackets denote thermal averages. The helicity modulus $\gamma_\perp$ measures the sensitivity of the system to an imposed infinitesimal angular gradient of the magnetic moments in the perpendicular direction. One of the most important consequences of a vortex dissociation is a jump from $\gamma_\perp(T_C^{XY}) = (2/\pi) k_B T_C^{XY}$ to zero just at $T_C^{XY}$.[30] In models of finite size the discontinuity is rounded out. However it turns out that the estimation of $T_C^{XY}$ from $\gamma_\perp$ is substantially less subject to finite-size shifts than, for instance, the determination of the critical temperature from the magnetization. Because the analysis of the spatially anisotropic two-dimensional (2D) $XY$ model within the framework of the self-consistent harmonic approximation[31] led to the conclusion that the jump in the helicity modulus depends on the anisotropy, the critical temperature was not extracted from the jump as has been conveniently done for the isotropic $XY$ model, but rather is defined by the temperature of the steepest decay in the helicity modulus. The other quantities recorded in our simulations were the total energy, the specific heat, and the susceptibility.

We have used a standard single spin-flip METROPOLIS algorithm[32] with periodic boundary conditions. During simulation we encountered convergence problems due to highly

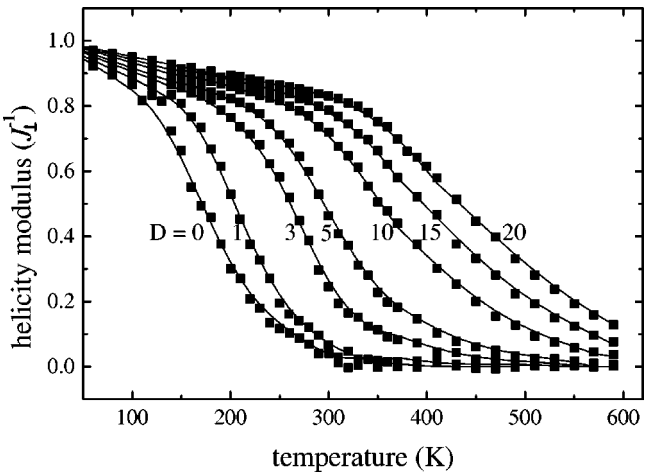


FIG. 3. The helicity modulus $\gamma_\perp$ as a function of temperature for different anisotropy parameters $D$.

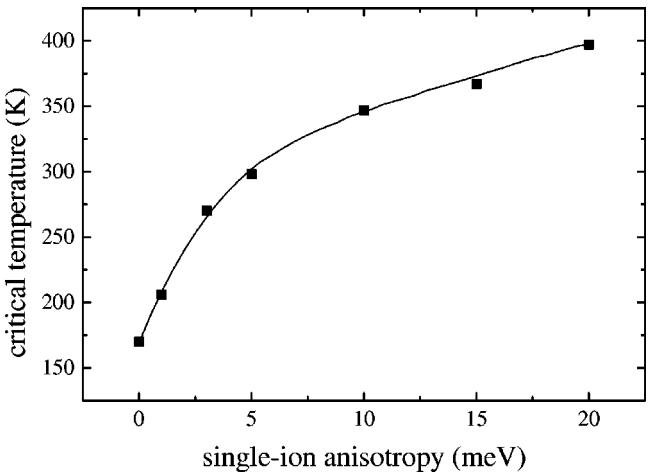


FIG. 4. The critical temperature of spatially anisotropic $XY$ model plotted versus the singe-ion anisotropy parameter $D$. The curve is a guide to the eye.

anisotropic exchange couplings. In particular, the tightly coupled atomic moments within a wire form large cluster moments interacting only weakly with neighboring large moments. This has repercussions on the time scale of flipping these huge moments, which is considerably longer than the time scale associated with fluctuating individual atomic moments. Only averages over as many as $4\times10^4$ Monte Carlo steps per lattice site per temperature gave reasonable accuracy. Such a slow convergence restricts the lattice size accessible by us to $20\times20$ sites. As our aim is not to pinpoint the critical temperature, the moderate lattice size is not an issue. The Monte Carlo simulations were performed for Fe wires on a Cu(117) surface, i.e., the chosen coupling constants were $J_\parallel=140.5$ meV, $J_\perp=3.9$ meV; the single-ion anisotropy $D$ assigned to all sites varied between 0 and 20 meV. Although a changed sign of $D$ will switch the easy axis, the critical temperature will not be affected.

The results for the temperature variation of $\gamma_\perp$ are plotted in Fig. 3. Critical temperatures are estimated from the maximum of the gradient in $\gamma_\perp(T)$. The dependence of the critical temperature on the anisotropy $D$ plotted in Fig. 4 demonstrates that despite a weak interwire coupling, the magnetic order of an array of Fe wires on Cu(117) persists at least to about 170 K. Obviously, the uniaxial anisotropy further stabilizes the ordered state. For the expected step-induced anisotropies of about 1 meV the system is supposed to disorder below room temperature, at about 210 K. We note that the critical temperatures derived from the inflection point of the magnetization as a function of $T$ are shifted by about 50 K upwards.

Next we turn to the nature of the phase transition. Since our simulations were done for models of a moderate size, sharp phase transitions cannot occur and smearing effects must be expected. The specific heat exhibits a broad rounded peak distinctly above the critical temperature, a trait typical for the $XY$ model. More eloquent evidence in favor of a phase-transition characteristic of the $XY$ model comes from the determination of the critical exponent $\beta$ describing the reduction of magnetization near $T_C$,

$$m=(T_C-T)^\beta, \quad T\rightarrow T_C. \tag{5}$$

In order to obtain the exponent $\beta$ we performed more extensive simulation on a $32\times32$ lattice taking $D=5$ meV. Our estimate of the critical exponent $\beta=0.24$ is in very good agreement with the value expected for the finite $XY$ model, $\beta=0.23$,[29] and differs substantially from the value of $\beta=0.125$ ensuing from the Ising model.

## VII. CONCLUSIONS

The purpose of this paper has been to outline, on theoretical grounds, the properties expected for one-dimensional magnetic structures. We have systematically studied the structural properties and magnetism of monatomic Fe wires on densely stepped Cu($11n$) surfaces for $n=3-11$ by means of a first-principles approach. The wires are straight and aligned parallel along the $\langle110\rangle$ direction. A single Fe wire suspended in vacuum assumes a warped zigzag-shaped form. The calculated equilibrium bond length of a free-standing straight wire is smaller by 12% than the corresponding bond length of a wire deposited on a Cu substrate. Hence, such a deposited wire is exposed to a significant tensile stress and thus it may be difficult to fabricate long continuous wires, or wires will not grow in registry with Cu template. Among the different locations of the wire on the stepped surface we have treated, the preferred position is at the inner corner sites, i.e., the sites with the highest coordination of Fe by Cu. Yet, at temperatures at which Fe atoms are still able to migrate on terraces, but the exchange processes necessary for incorporating Fe in the host are kinetically inhibited, a formation of wires attached to the steps is predicted.

By comparing the total energies of ferromagnetic and antiferromagnetic configurations, the intrawire and interwire magnetic coupling constants were obtained. We have found a ferromagnetic order in all models under consideration, namely, for interwire separations between 4.1 and 14.2 Å. A reversal to an antiferromagnetic order at larger separations

cannot be excluded, though. Provided that the shape anisotropy is efficient to fix the magnetic moments in a $(11n)$ plane, the calculated magnetic interaction parameters can be used as input for a Monte Carlo simulation of a pertinent 2D $XY$ model. The presence of a step-induced anisotropy of unknown strength has been taken into account through a single-ion anisotropy term. The treatment of rounding phenomena by means of a finite-size scaling analysis would require going to bigger models. Nevertheless, our critical temperatures of 200–300 K for anisotropies of 1–5 meV can be taken as reasonable estimates.

The spontaneous magnetization was found to vanish following a power-law behavior with a characteristic exponent of $\beta = 0.24$. This value is a universal signature of finite 2D $XY$ critical behavior. Hence it appears that a weak uniaxial anisotropy is a marginal variable, i.e., it does not influence the critical behavior, or the crossover region to an Ising behavior is too narrow to be accessible in our simulations.

## ACKNOWLEDGMENTS

This work has been supported by the Austrian Science Funds within Project No. P12753, ''Magnetism on the nanometer scale,'' and through the Center for Computational Materials Science.

*Email address: Daniel.Spisak@univie.ac.at

[1] F.J. Himpsel, J.E. Ortega, G.J. Mankey, and R.F. Willis, Adv. Phys. **47**, 511 (1998).
[2] A. Fert and L. Piraux, J. Magn. Magn. Mater. **200**, 338 (1999).
[3] D.J. Sellmyer, M. Zheng, and R. Skomski, J. Phys.: Condens. Matter **13**, R433 (2001).
[4] Y. Zhang and Hongjie Dai, Appl. Phys. Lett. **77**, 3015 (2000).
[5] H.J. Elmers, J. Hauschild, H. Höche, U. Gradmann, H. Bethge, D. Heuer, and U. Köhler, Phys. Rev. Lett. **73**, 898 (1994).
[6] T. Jung, R. Schlittler, J.K. Gimzewski, and F.J. Himpsel, Appl. Phys. A: Mater. Sci. Process. **A61**, 467 (1995).
[7] J. Shen, R. Skomski, M. Klaua, H. Jenniches, S. Sundar Manoharan, and J. Kirschner, Phys. Rev. B **56**, 2340 (1997).
[8] V. Repain, J.M. Berroir, S. Rousset, and J. Lecoeur, Surf. Sci. **447**, L152 (2000).
[9] P. Gambardella, M. Blanc, H. Brune, K. Kuhnke, and K. Kern, Phys. Rev. B **61**, 2254 (2000).
[10] P. Gambardella, M. Blanc, L. Bürgi, K. Kuhnke, and K. Kern, Surf. Sci. **449**, 93 (2000).
[11] J.-L. Lin, D.Y. Petrovykh, A. Kirakosian, H. Rauscher, and F.J. Himpsel, Appl. Phys. Lett. **78**, 829 (2001).
[12] V. Bellini, N. Papanikolaou, R. Zeller, and P.H. Dederichs, Phys. Rev. B **64**, 094403 (2001).
[13] D. Spišák, Surf. Sci. **489**, 151 (2001).
[14] M. Giesen, C. Steimer, and H. Ibach, Surf. Sci. **471**, 80 (2000).
[15] F. Dulot, B. Kierren, and D. Malterre, Surf. Sci. **494**, 229 (2001).
[16] G. Kresse and J. Furthmüller, Phys. Rev. B **54**, 11 169 (1996); Comput. Mater. Sci. **6**, 15 (1996).
[17] P. Blöchl, Phys. Rev. B **50**, 17 953 (1994).
[18] G. Kresse and D. Joubert, Phys. Rev. B **59**, 1758 (1999).
[19] J. Perdew and A. Zunger, Phys. Rev. B **23**, 5048 (1981).
[20] S.H. Vosko, L. Wilk, and M. Nusair, Can. J. Phys. **58**, 1200 (1980).
[21] J.P. Perdew, J.A. Chevary, S.H. Vosko, K.A. Jackson, M.R. Pedersen, D.J. Singh, and C. Fiolhais, Phys. Rev. B **46**, 6671 (1992).
[22] C. Kittel, *Introduction to Solid State Physics*, 7th ed. (Wiley, New York, 1996), p. 300.
[23] D. Spišák and J. Hafner, Phys. Rev. B **64**, 205422 (2001).
[24] D. Spišák and J. Hafner, J. Magn. Magn. Mater. **168**, 257 (1997).
[25] L. Onsager, Phys. Rev. **65**, 117 (1944).
[26] D. Spišák, J. Magn. Magn. Mater. **132**, 311 (1994).
[27] Y.Q. Ma, Phys. Lett. A **225**, 311 (1997).
[28] J.M. Kosterlitz and D.J. Thouless, J. Phys. C **6**, 1181 (1973).
[29] S.T. Bramwell and P.C.W. Holdsworth, J. Phys.: Condens. Matter **5**, L53 (1993).
[30] D.R. Nelson and J.M. Kosterlitz, Phys. Rev. Lett. **39**, 1201 (1977).
[31] D. Spišák, Physica B **190**, 407 (1993).
[32] For a review see, e.g., *Monte Carlo Methods in Statistical Physics*, edited by K. Binder (Springer, New York, 1979).